

Article

Electrospun ZnSnO₃/ZnO Composite Nanofibers and Its Ethanol-Sensitive Properties

Songtao Dong^{1,2,*}, Xiaoyun Jin², Junlin Wei² and Hongyan Wu^{1,*}

¹ Institute of Advanced Materials and Flexible Electronics (IAMFE), School of Chemistry and Materials Science, Nanjing University of Information Science and Technology, Nanjing 210044, China

² Institute of Material Science and Engineering, Jiangsu University of Science and Technology, Zhenjiang 212003, China; xiaoyunjin2021@126.com (X.J.); 182060012@stu.just.edu.cn (J.W.)

* Correspondence: stdong@just.edu.cn (S.D.); wuhy2009@nuist.edu.cn (H.W.)

Abstract: In this work, a novel heterojunction based on ZnSnO₃/ZnO nanofibers was prepared by a simple electrospinning method. The crystal, structural, and surface compositional properties of ZnSnO₃ and ZnSnO₃/ZnO composite nanofibers were investigated by X-ray diffractometer (XRD), scanning electron microscope (SEM), transmission electron microscope (TEM), X-ray photoelectron spectrometer (XPS), and Brunauer–Emmett–Teller (BET). Compared to pure ZnSnO₃ nanofibers, the ZnSnO₃/ZnO heterostructure nanofibers had high sensitivity and selectivity response with the fast response toward ethanol gas at low operational temperature. The sensing response of the sensor based on ZnSnO₃/ZnO composite nanofibers was 19.6 toward 50 ppm ethanol gas at 225 °C, which was about 1.5 times superior to that of pure ZnSnO₃ nanofibers. It can be owed mainly to the oxygen vacancies and the synergistic effect between ZnSnO₃ and ZnO.

Keywords: electrospinning; ZnSnO₃/ZnO nanofibers; sensing performance; n-n heterojunction



Citation: Dong, S.; Jin, X.; Wei, J.; Wu, H. Electrospun ZnSnO₃/ZnO Composite Nanofibers and Its Ethanol-Sensitive Properties. *Metals* **2022**, *12*, 196. <https://doi.org/10.3390/met12020196>

Academic Editor: Asit Kumar Gain

Received: 4 January 2022

Accepted: 19 January 2022

Published: 21 January 2022

Publisher's Note: MDPI stays neutral with regard to jurisdictional claims in published maps and institutional affiliations.



Copyright: © 2022 by the authors. Licensee MDPI, Basel, Switzerland. This article is an open access article distributed under the terms and conditions of the Creative Commons Attribution (CC BY) license (<https://creativecommons.org/licenses/by/4.0/>).

1. Introduction

In recent years, with the increasing demand for the detection of toxic gases, volatile organic compounds, and clinical gas analysis, gas sensor research has become more extensive. High sensitivity, fast response, excellent selectivity, and long-term stability are the basic parameters of the highly sensitive gas sensors [1]. Semiconductor metal oxide gas sensors have attracted widespread attention due to their advantages such as fast response, low cost, simple structure, and good compatibility. Semiconductor metal oxide materials (e.g., NiO [2], SnO₂ [3,4], ZnO [5], CuO [6], etc.) are widely used for their high performance, cost-effectiveness, and excellent gas-sensing properties. Still, these binary oxide materials operate at high temperatures, so the search for a sensing material with low operating temperature and high sensitivity has become a focus of current research.

At present, ternary transition metal oxides as new gas-sensitive materials have received widespread attention due to their excellent gas-sensitive properties, structural stability, especially their unique energy band structure, and unique physical and chemical properties. However, due to its low exposure area and low electron transfer, many ternary metal oxides tend to show lower gas sensitivity [7]. Among the ternary tin-based metal oxides, ZnSnO₃ is a typical perovskite structure oxide material with Zn at the A-site and Sn at the B-site. Compared to ZnO and SnO₂, ZnSnO₃ has been widely used in gas sensors for its high chemical sensitivity and excellent electrical properties [8]. The spatial arrangement of the atoms in the ZnSnO₃ system is an octahedron. The unique crystal structure of ZnSnO₃ has a lot of oxygen vacancies, providing more oxygen adsorption sites, which can promote the reaction with reducing gases, thus improving gas sensitivity [8]. Many studies have focused on single-component ZnSnO₃ as a gas sensing material. Wang et al. [9] reported that the sensing response to 100 ppm H₂S of hollow, cubic-structured ZnSnO₃ samples were up to 1418 at an optimum operating temperature of 335 °C. ZnSnO₃ nanomicrospheres

were prepared by the hydrothermal method, which had high selectivity for n-butanol at 200 °C [10]. Wang et al. found that ZnSnO₃ samples prepared by co-precipitation and heat treatment had a high sensing response to ethanol, reaching 147 [11]. Researchers have also designed heterogeneous structures to improve the gas-sensing performance, such as ZnSnO₃/TiO₂, SnO₂/TiO₂, WO₃/SnO₂, and ZnSnO₃/ZnO [12–15]. To further improve the gas-sensitive performance of ZnSnO₃, Yu et al. [16] compounded ZnSnO₃ with CuO and found a sensing response to ethanol of up to 131. Zhang et al. [17] and Cheng et al. [18] reported that ZnSnO₃ was compounded with SnO₂; due to the excellent physical and chemical properties of both SnO₂ and ZnSnO₃, the gas-sensitive properties of the SnO₂/ZnSnO₃ composite were significantly improved compared to both SnO₂ and ZnSnO₃ materials. The cubic ZnSnO₃/ZnO heterostructure showed a much improved response to 50 ppm triethylamine compared to pure ZnSnO₃ ($R_a/R_g = 21$) [15]. These results indicated that heterostructures composed of MO_x and ZnSnO₃ had great potential for gas-sensing applications.

Currently, researchers have prepared ZnSnO₃ nanofibers with different morphologies (e.g., spherical, polyhedral, etc.) [19,20], but there are few reports on nanofiber samples with ZnSnO₃-based heterojunctions. The electrospinning method can obtain nanofiber materials with high specific surface area and different morphologies. Based on the above considerations, ZnSnO₃ nanofibers and ZnSnO₃/ZnO composite nanofibers were synthesized by electrospinning in this paper. The results of gas-sensitive performance of ZnSnO₃ nanofibers and ZnSnO₃/ZnO nanofibers showed that the ZnSnO₃/ZnO nanofibers had a lower operating temperature (225 °C), a sensitivity response of 19.6 at 50 ppm in ethanol atmosphere, and better stability than ZnSnO₃. A possible enhanced gas-sensing mechanism was proposed.

2. Experimental Section

2.1. Material Preparation

A combination of electrospinning and calcination was used to prepare ZnSnO₃/ZnO nanofibers. The experimental procedure was as follows: First, appropriate amounts of stannous chloride (SnCl₂·2H₂O) and zinc chloride (ZnCl₂) were dissolved in a mixed solution of 8 g N, N-dimethylformamide (DMF) and 12 g anhydrous ethanol under constant stirring so that the molar ratio of Sn⁴⁺ to Zn²⁺ was 1:1.2. Next, 2 g of polyvinylpyrrolidone (PVP; average molecular weight of 1,300,000 g·mol⁻¹) was added and stirred thoroughly to finally obtain the precursor solution required for the electrospinning method. Then, the electrospinning precursor solution was loaded into a plastic syringe with a 22-gauge needle, and the advance rate of the syringe pump was set at 0.4 mL·h⁻¹. A voltage of 15 kV was applied between the needle and the collector, and a layer of aluminum foil was wrapped around the rotating receiver 20 cm from the needle to collect the fibers. The collected precursor fibers were calcined in air at 450 °C for 2 h to obtain ZnSnO₃/ZnO nanofibers.

2.2. Characterization

The physical phases of the calcined samples were analyzed by X-ray powder diffractometer (XRD, Bruker D8 Advance, Bruker, Billerica, MA, USA) using a copper target K_α line with a scanning range of 20–60° and a scanning speed of 6°/min. The field-emission scanning electron microscopy (FESEM; Merlin Compact, Carl Zeiss AG, Oberkochen, Germany) and transmission electron microscope (TEM; JEOL 2100F, JEOL Ltd., Tokyo, Japan) were used to characterize the morphology of the samples. Thermogravimetric (TG) tests were carried out by a thermal analysis system (Diamond TG/DTA, Perkin Elmer S. A., Waltham, MA, USA) to determine the calcination temperature of the precursors. The weight of the sample was 4–6 mg during the test, and it was heated to 600 °C at a heating rate of 15 °C/min. The elemental composition and valence states in the material were characterized using an X-ray photoelectron spectrometer (Thermo Scientific K-Alpha, XPS, Thermo Fisher Scientific, Waltham, MA, USA). The specific surface area of the prepared nanofibers was

tested by Brunner–Emmet–Teller (BET, Micromeritics ASAP 2020, Micromeritics Instrument Corporation, Norcross, GA, USA).

2.3. Gas-Sensitive Performance Measurement

A 200 mg sample of ZnSnO₃/ZnO nanofibers was mixed well with 0.2 mL of deionized water in an agate mortar and ground to a paste. Then, the ground paste sample was uniformly coated on the surface of the Ag-Pd forked finger electrode on an Al₂O₃ substrate and dried for a certain period of time to obtain the gas-sensitive element required for the test. Before testing, the dried gas-sensitive components were aged in the air for 10 h. The sensitivity response, operating temperature, and stability of the preparations were tested on the CGS-1TP Intelligent Gas Sensitive Analysis System (Beijing Elite Technology Co., Ltd., Beijing, China).

3. Results and Discussion

3.1. Microstructure and Morphology

To determine the calcination temperature of the ZnSnO₃ precursor obtained by electrospinning methods, TG tests were carried out on the ZnSnO₃ precursor under an air atmosphere in the temperature range of 30–600 °C with a heating rate of 15 °C/min; the results are shown in Figure 1a. Figure 1a shows an 8 wt % drop in sample mass at 300 °C. This is due to the evaporation of organic solvents and the evaporation of gases and moisture adsorbed on the surface of the ZnSnO₃ precursor. The sharp decrease in sample mass around 350 °C can be attributed to the decomposition of the precursor, while the significant drop in the curve around 400 °C can be attributed to the decomposition of PVP. In addition, no significant weight changes are observed above 450 °C, which proves that all organic matter in the precursor decomposes at 450 °C and that calcination of the precursor at temperatures higher than 450 °C is sufficient. Figure 1b shows the XRD results of the ZnSnO₃ and ZnSnO₃/ZnO precursors after 2 h of calcination at 450 °C. A comparison with the standard card (PDF No. 28–1486) shows that the XRD diffraction peaks at 2θ of 26.5°, 33.7°, 37.7°, 51.6°, and 54.6° correspond to the (012), (110), (015), (116), (018), and (214) crystal planes of the ZnSnO₃, respectively. The remaining XRD diffraction peaks are compared with the standard card (PDF No. 65–3411) and are found to correspond to (100), (101), (102), and (110) crystal planes at 2θ of 31.7°, 36.3°, 47.5°, and 56.6°, respectively. The XRD diffraction peak corresponding to the standard card (PDF No. 65–3411) is the diffraction peak of ZnO. The results show that ZnSnO₃ and ZnSnO₃/ZnO nanofibers are successfully synthesized after calcination in air at 450 °C for 2 h.

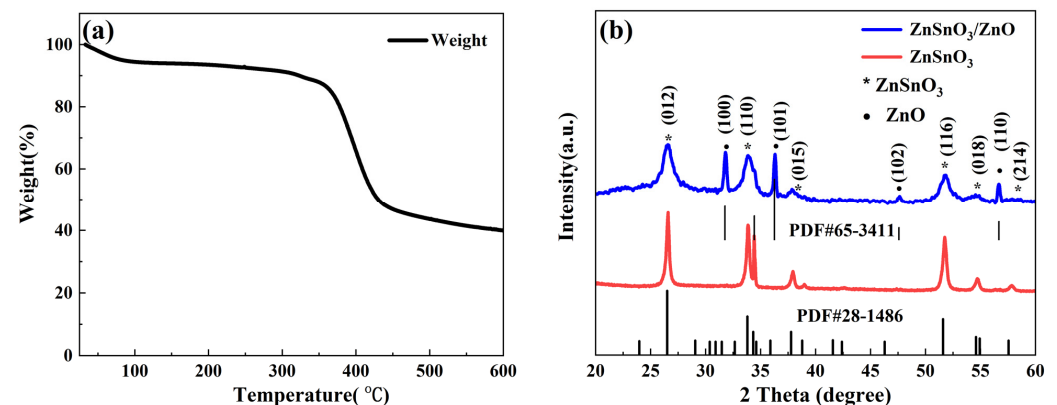


Figure 1. (a) TG results of ZnSnO₃ precursors; (b) XRD patterns of ZnSnO₃ and ZnSnO₃/ZnO calcined at 450 °C.

Figure 2a,b show the SEM results of the ZnSnO₃ samples prepared after calcination at 450 °C for 2 h in an air atmosphere. From Figure 2a, the ZnSnO₃ samples after calcination at 450 °C for 2 h in an air atmosphere are coarse and uniformly fibrous, with no breakage of the continuous fibers. The average diameter of the ZnSnO₃ sample is about

300–400 nm, as shown in Figure 2b. Figure 2c,d show the SEM results of ZnSnO₃/ZnO samples prepared after calcination at 450 °C for 2 h in an air atmosphere. As can be seen in Figure 2c, the ZnSnO₃/ZnO samples exhibit uniformly coarse and fine fibers with no fracture in the fiber continuity. The average diameter of the ZnSnO₃/ZnO nanofibers is even smaller, around 200 nm, as shown in Figure 2d. The TEM image in Figure 2d indicates that the ZnSnO₃/ZnO nanofibers have a hollow structure. According to the results of Li et al. [21], the morphology of nanofibers or nanotubes is mainly dependent on the calcination temperature. During calcination, PVP is gradually removed as the temperature increases. The decomposition of the drug and the evaporation of the solvent will generate a variety of gases. When the calcination temperature reaches 450 °C, the rate of gas production from the decomposition of pharmaceuticals is too fast, and the pressure difference between the interior and exterior of the nanofibers is more considerable, so the hollow structure is formed [21]. The above experiments show that the diameter of the ZnSnO₃/ZnO nanofibers obtained by compounding ZnSnO₃ with ZnO is significantly reduced compared to the ZnSnO₃ nanofiber samples. The BET analysis shows that the specific surface area of the ZnSnO₃/ZnO nanofibers (31.24 m²·g⁻¹) was substantially larger than that of pristine ZnSnO₃ nanofibers (20.15 m²·g⁻¹), as shown in Figure 2e,f.

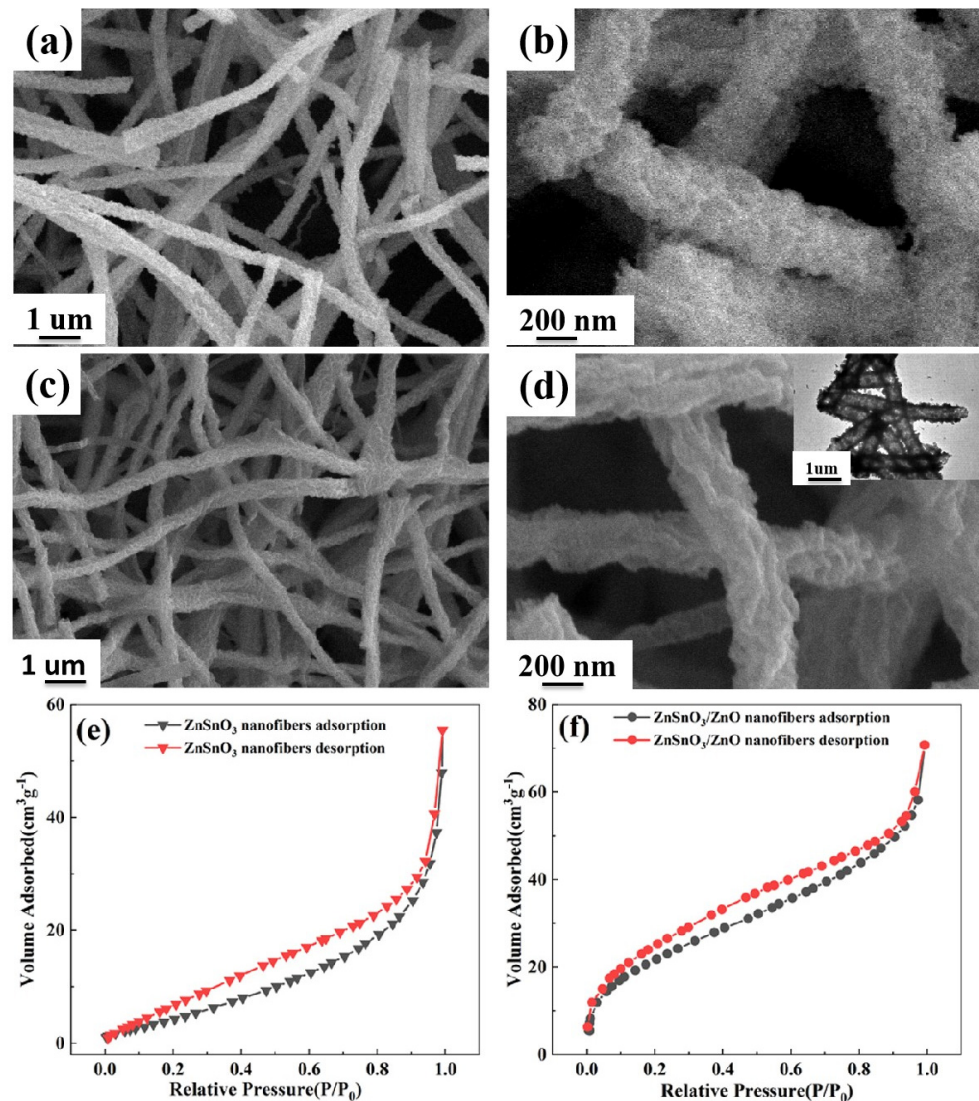


Figure 2. SEM images of ZnSnO₃ and ZnSnO₃/ZnO: (a,b) ZnSnO₃, (c,d) ZnSnO₃/ZnO, the inset in (d) TEM image of ZnSnO₃/ZnO; (e,f) N₂ adsorption–desorption isotherms of ZnSnO₃ and ZnSnO₃/ZnO nanofibers.

XPS is carried out to study the elemental composition and valence states in ZnSnO₃/ZnO, and the results are shown in Figure 3. Figure 3a shows the full XPS spectrum of the ZnSnO₃/ZnO nanofibers; we can observe that the obtained ZnSnO₃/ZnO nanofibers contain the elements Zn, Sn, C, and O. The peak at 284.8 eV corresponds to the spin-orbit peak of C 1s. The broad XPS spectrums of the Zn 2p range, Sn 3d, and O 1s range are shown in Figure 3b–d. In the case of the Zn 2p spectrum, the Zn 2p peak can be distributed into two signals, as shown in Figure 3b. The Zn-2p_{3/2} and Zn-2p_{1/2} signals are focused at 1021.1 eV and 1044.1 eV, respectively, which indicates that the chemical valence of Zn in the system is +2 [22]. As shown in Figure 3c, the two peaks at 486.8 and 495.1 eV correspond to the Sn 3d_{5/2} and Sn 3d_{3/2} spin-orbit peaks, respectively. The bimodal spin-orbit shows a split value of approximately 8.3 eV, indicating the presence of Sn⁴⁺ cations [23]. The O 1s spectrum of the ZnSnO₃ and ZnSnO₃/ZnO is illustrated in Figure 3d,e, which is deconvoluted into three characteristic peaks by Gaussian fitting [16,24]. The three fitting peaks are attributed to three essential oxygen species [25], which are denoted as O_L, O_V, and O_C, respectively, corresponding to O²⁻ species in the lattice oxygen species, vacancy oxygen species (VO_S), and chemically adsorbed or dissociated oxygen species, respectively [26]. The three characteristic peaks of O 1s in the ZnSnO₃ nanofibers are located at 530.06 eV, 531.65 eV, and 533.13 eV. In contrast, the distinct peaks of O 1s in the ZnSnO₃/ZnO nanofibers are located at 529.99 eV, 531.33 eV, and 532.27 eV, which can be ascribed to the three significant oxygen species, represented as O_L, O_V, and O_C, respectively [17,27]. It must be pointed out that the gas-sensing properties may be highly dependent on the type of VO (vacancy oxygen) present on the semiconductor surface [28]. The proportion of oxygen species in the obtained ZnSnO₃ and ZnSnO₃/ZnO nanofibers are shown in Figure 3f and Table 1. The results of Figure 3f and Table 1 clearly indicate that compared with the percentage of O_V of ZnSnO₃ nanofibers, that of ZnSnO₃/ZnO nanofibers is substantially larger.

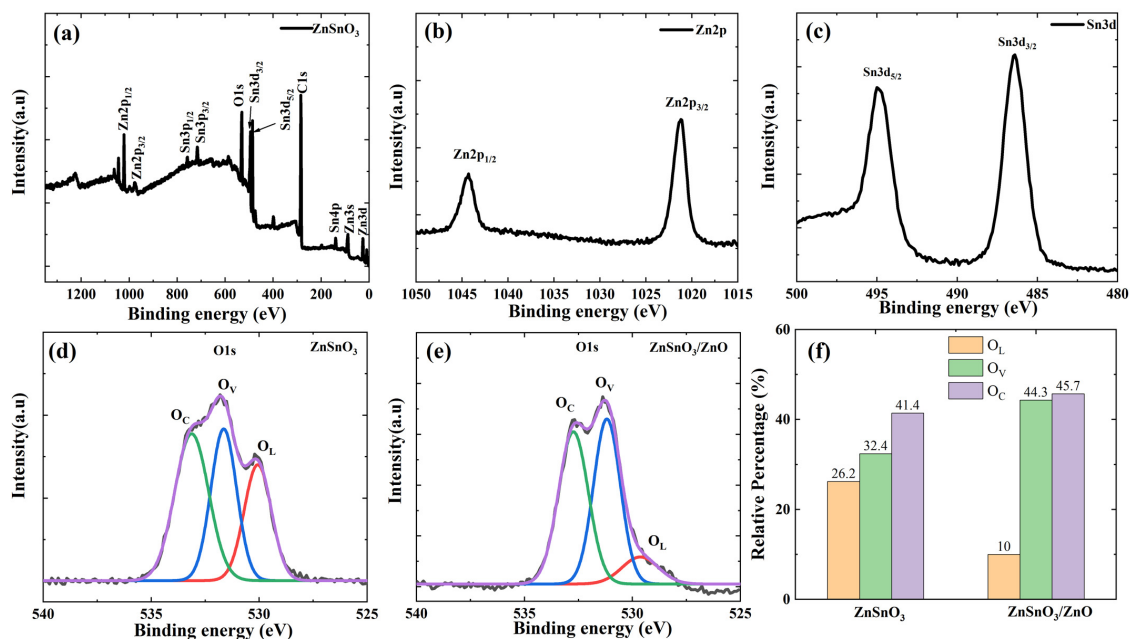


Figure 3. XPS spectra of ZnSnO₃/ZnO nanofibers: (a) a survey spectrum, high-resolution spectra for (b) Zn 2p, (c) Sn 3d, (d) O 1s (of ZnSnO₃), (e) O 1s (of ZnSnO₃/ZnO), (f) fitting results of O 1s XPS spectra of ZnSnO₃ and ZnSnO₃/ZnO.

Table 1. The proportion of oxygen species in obtained ZnSnO₃ and ZnO/ZnSnO₃ nanofibers.

Sample	O _L (%)	O _V (%)	O _C (%)
ZnSnO ₃	26.2%	32.4%	41.4%
ZnSnO ₃ /ZnO	10%	44.3%	45.7%

3.2. Gas-Sensitive Performances of ZnSnO₃/ZnO Nanofibers

It is well known that changes in operating temperature can highly influence the gas-sensing performances of sensing materials. To verify this, the response of the ZnSnO₃ nanofibers and ZnSnO₃/ZnO composite nanofibers toward 50 ppm ethanol gas is tested at different temperatures, and the results are shown in Figure 4. For n-type devices, the response value (S) of the reducing gas sensors are defined as $S = R_a/R_g$, where R_a is the resistance of the sensor in air, and R_g is the resistance of the device in the target gases.

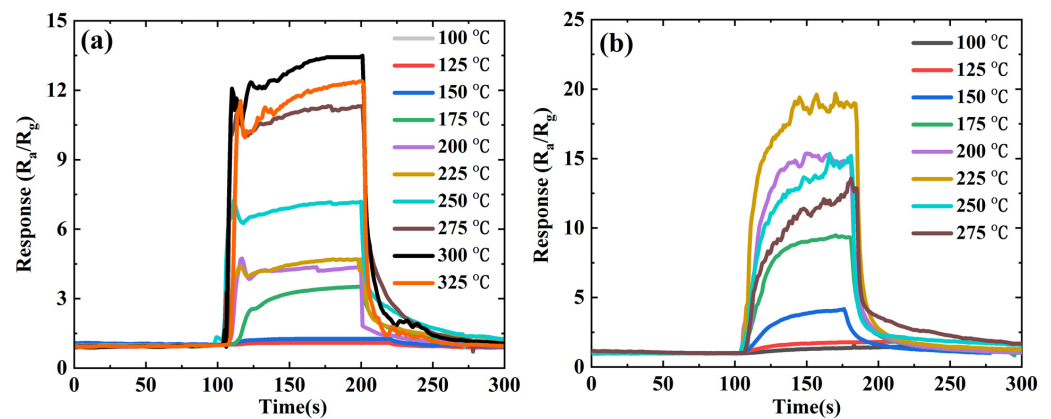


Figure 4. Response of ZnSnO₃ and ZnSnO₃/ZnO toward 50 ppm ethanol at different temperatures: (a) ZnSnO₃; (b) ZnSnO₃/ZnO.

Figure 4a shows that the response of the ZnSnO₃ sample increases with increasing temperature until the temperature rises to 300 °C; the maximum response value is 13.4. Then, as temperature increases, the response decreases. Figure 4b shows the sensing response of the ZnSnO₃/ZnO composite nanofibers toward 50 ppm ethanol gas at different temperatures. The results show that the optimum operating temperature and the maximum sensing response value for ZnSnO₃/ZnO composite nanofibers are 225 °C and 19.6, respectively. The optimum operating temperature of the ZnSnO₃/ZnO composite nanofibers is significantly lower than that of the ZnSnO₃ nanofibers. The sensing response has also been improved, with a 46.3% increase in the sensing response.

To further investigate the gas-sensing performance of the ZnSnO₃/ZnO composite nanofibers, the response of the ZnSnO₃ and ZnSnO₃/ZnO nanofibers in the different concentrations of ethanol and the stability of the response to 50 ppm ethanol was tested at the optimum operating temperature, respectively. The results are shown in Figure 5. As shown in Figure 5a, the response of the ZnSnO₃ nanofibers increases with increasing ethanol concentration because with increasing ethanol concentration, more ethanol molecules react with the oxygen ions adsorbed on the surface of the material, resulting in a higher carrier concentration and thus a subsequent increase in the response of the material. Figure 5b shows that the response of the ZnSnO₃/ZnO composite nanofibers increases with increasing ethanol concentration. In contrast, the response of the ZnSnO₃/ZnO samples is higher than that of the ZnSnO₃ samples at the same concentration of ethanol.

Figure 5c,d show the response stability of the ZnSnO₃ sample and the ZnSnO₃/ZnO samples under ethanol atmosphere at 50 ppm, respectively. As can be seen from Figure 5c,d, the ZnSnO₃ and ZnSnO₃/ZnO samples show no significant fluctuations in response after six repeated exposures to ethanol at 50 ppm, indicating that both the ZnSnO₃ and ZnSnO₃/ZnO samples have good stability. The above experimental results show that the ZnSnO₃/ZnO samples have a lower working temperature, higher response, and better stability for ethanol atmosphere than that of the ZnSnO₃ samples.

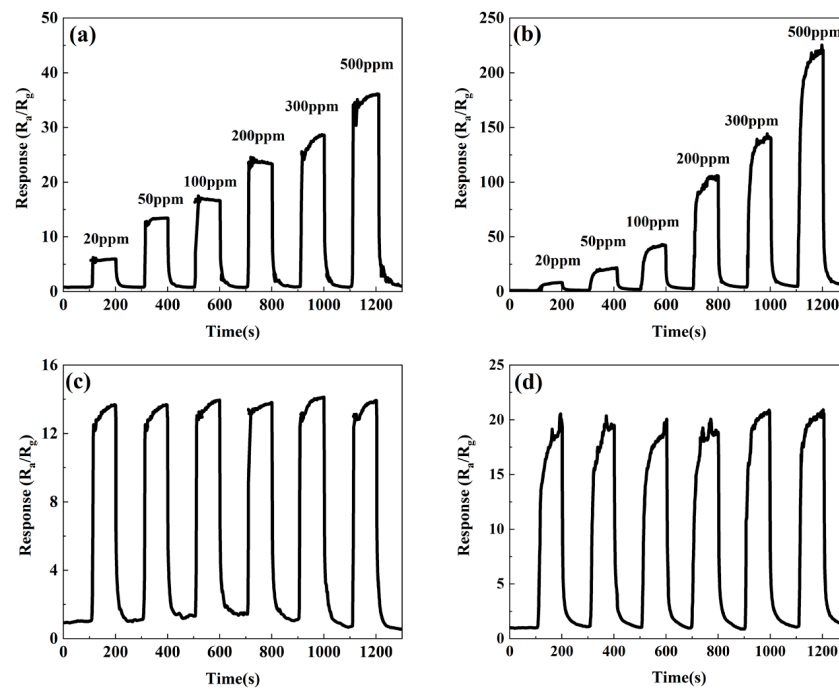
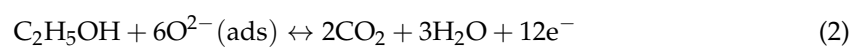
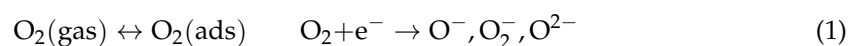


Figure 5. Response of ZnSnO₃ and ZnSnO₃/ZnO to different concentrations of ethanol at the optimal working temperature: (a) ZnSnO₃; (b) ZnSnO₃/ZnO; the stability of response to 50 ppm ethanol at optimum operating temperature: (c) ZnSnO₃; (d) ZnSnO₃/ZnO.

3.3. Gas-Sensing Mechanism

The sensing mechanism based on the metal oxide semiconductor gas sensor is the changed resistance caused by the adsorption and desorption of the target gas molecules on the surface of sensing materials, which depends mainly on the concentration and mobility of the charge. Therefore, the gas-sensitive mechanism of the ZnSnO₃ and ZnSnO₃/ZnO composite nanofibers can be understood simply as a surface-controlled mechanism. The change in resistance depends on the type and amount of oxygen chemisorbed on the surface. In air atmosphere, the resistance of ZnSnO₃ and ZnSnO₃/ZnO composite nanofibers is primarily controlled by the concentration of adsorbed oxygen (O⁻, O₂⁻, and O²⁻). The variation in response for ZnSnO₃ nanofibers is mainly related to the adsorption–desorption reaction of ethanol gas on the surface of ZnSnO₃ samples. ZnSnO₃ is a typical N-type semiconductor material, when it is in the air, oxygen molecules adsorbed on the surface of ZnSnO₃ gain electrons and thus convert into O⁻, O₂⁻, and O²⁻ ions (Equation (1)). When a certain amount of oxygen ions accumulated on the material surface reaches equilibrium, an electron depletion layer (EDL) is formed on the material surface, which results in a high sensor resistance (R_a) and a relatively high potential barrier, as shown in Figure 6a. However, when ZnSnO₃ is placed in an ethanol atmosphere, the ethanol molecules react with oxygen ions (Equation (2)). As shown in Figure 6b, the consequent decrease in potential barrier height and the narrowing of the EDL width result in a reduction of the sensor resistance (R_g). The equations for the above process reaction are as follows [29]:



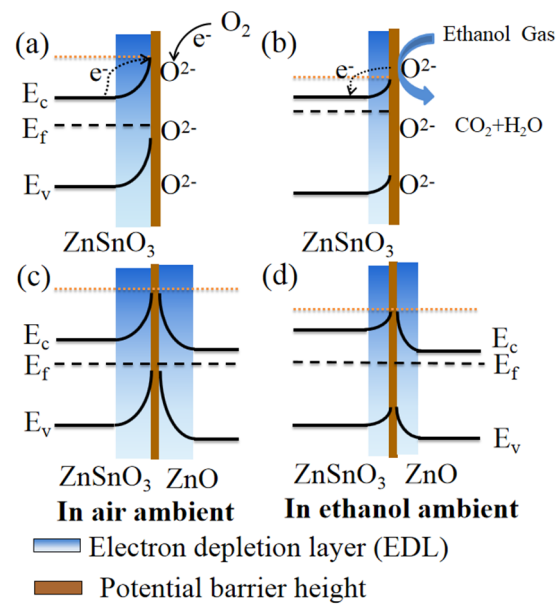


Figure 6. Schematic illustration for the variation of EDL width and potential barrier height: (a) and (b): ZnSnO₃; (c) and (d) ZnSnO₃/ZnO exposed to air and ethanol, respectively.

According to reference [15], since both ZnSnO₃ and ZnO are N-type semiconductor materials, ZnO is successfully compounded with ZnSnO₃ to form a homotypic heterojunction (i.e., N-N junction); this N-N junction is a critical factor in improving the ethanol gas sensitivity between ZnSnO₃ and ZnO. There were differences in the Fermi energy levels of the two connected semiconductor compounds. The transfer of electrons from higher energy states to lower energy states until equilibrium is reached at the Fermi energy level resulted in the formation of a depletion layer in the interface region. In contrast to ZnSnO₃, the electrons on the ZnSnO₃ conduction band in the ZnSnO₃/ZnO sample are transferred to the ZnO conduction band to be trapped by oxygen molecules, resulting in the formation of a large number of oxygen anions. At the same time, the electron depletion layer appears near the surface of ZnSnO₃/ZnO, which is an essential component of the gas-sensing process. In an air environment, the increased height of the potential barrier of the ZnSnO₃/ZnO heterostructured composite makes electron transfer more difficult (as shown in Figure 6c), which also leads to a significant increase in sensor resistance (R_a). In an ethanol environment, the reaction of ethanol molecules with oxygen ions releases electrons back into the ZnSnO₃/ZnO heterojunction, resulting in an increase in electron concentration. This reduces the potential barrier height of ZnSnO₃ and ZnO, considerably reducing the sensor resistance (R_g), as shown in Figure 6d. The analysis of the above gas-sensitive properties reveals that compared to the ZnSnO₃ nanofibers, the heterogeneous structure of the ZnSnO₃/ZnO composite nanofibers enhances electron transport and enables the effective separation of electrons and holes. According to Equation (1) and Equation (2), the larger specific surface area of ZnSnO₃/ZnO facilitates the adsorption of more oxygen on its surface, producing a large amount of oxygen ions, thus resulting in higher sensor resistance (R_a) and the lower sensor resistance (R_g). So, the gas-sensing response of ZnSnO₃/ZnO composite nanofibers increases.

Compared to ZnSnO₃ nanofibers, ZnSnO₃/ZnO composite nanofibers have a larger VOs of 44.3%, which is almost 1.5 times that of ZnSnO₃ nanofibers, which is conducive to improving the sensing performance of gas-sensitive materials [30]. It is also suggested that in the “chemical sensitization” mechanism established by the spillover effect, ZnO plays a vital role in activating the dissociation rate of molecular oxygen [31].

4. Conclusions

In conclusion, ZnSnO₃ nanofibers and ZnSnO₃/ZnO composite nanofibers were successfully prepared using a simple electrospinning method. The average diameter of the ZnSnO₃/ZnO composite nanofibers was approximately 200 nm. Compared to ZnSnO₃ nanofibers, ZnSnO₃/ZnO nanofibers had a lower operating temperature (225 °C), higher response (19.6), and better stability in an ethanol atmosphere, which can be owed mainly to the presence of oxygen vacancies and the synergistic effect between ZnSnO₃ and ZnO. The results confirmed that the ZnSnO₃/ZnO nanofibers could be an outstanding potential candidate for ethanol detection.

Author Contributions: Conceptualization and data curation, S.D.; methodology and formal analysis, X.J.; investigation, J.W.; writing—original draft preparation, S.D.; writing—review and editing, H.W. All authors have read and agreed to the published version of the manuscript.

Funding: This research was funded by the National Natural Science Foundation of China (Grant No. 51702132) and the Postgraduate Research & Practice Innovation Program of Jiangsu Province (Grant No. KYCX20_3132).

Data Availability Statement: Not applicable.

Acknowledgments: The authors acknowledge financial support from the National Natural Science Foundation of China (51702132). Song-Tao Dong acknowledges the open project of the National Laboratory of Solid State Microstructures at Nanjing University. Jun-Lin Wei acknowledges financial support from the Postgraduate Research & Practice Innovation Program of Jiangsu Province (Grant No. KYCX20_3132).

Conflicts of Interest: The authors declare no conflict of interest.

References

1. Ma, J.; Xiao, X.; Zou, Y.; Ren, Y.; Zhou, X.; Yang, X.; Cheng, X.; Deng, Y. A general and straightforward route to noble metal-decorated mesoporous transition-metal oxides with enhanced gas sensing performance. *Adv. Funct. Mater.* **2019**, *15*, e1904240. [[CrossRef](#)]
2. Goma, M.M.; Sayed, M.H.; Patil, V.L.; Boshta, M.; Patil, P.S. Gas sensing performance of sprayed NiO thin films toward NO₂ gas. *J. Alloys Compd.* **2021**, *885*, 160908. [[CrossRef](#)]
3. Wang, Y.; Zeng, Y.; Wang, L.; Lou, Z.; Qiao, L.; Tian, H.; Zheng, W. Ultrathin nanorod-assembled SnO₂ hollow cubes for high sensitive n-butanol detection. *Sens. Actuators B Chem.* **2019**, *283*, 693–704. [[CrossRef](#)]
4. Kou, X.; Xie, N.; Chen, F.; Wang, T.; Guo, L.; Wang, C.; Wang, Q.; Ma, J.; Sun, Y.; Zhang, H.; et al. Superior acetone gas sensor based on electrospun SnO₂ nanofibers by Rh doping. *Sens. Actuators B Chem.* **2018**, *256*, 861–869. [[CrossRef](#)]
5. Kim, J.H.; Mirzaei, A.; Kim, H.W.; Kim, S.S. Low voltage driven sensors based on ZnO nanowires for room temperature detection of NO₂ and CO gases. *ACS Appl. Mater. Interfaces* **2019**, *1*, 24172–24183. [[CrossRef](#)]
6. Geng, W.; Ma, Z.; Yang, J.; Duan, L.; Li, F.; Zhang, Q. Pore size dependent acetic acid gas sensing performance of mesoporous CuO. *Sens. Actuators B Chem.* **2021**, *334*, 129639. [[CrossRef](#)]
7. Jain, K.; Pant, R.P.; Lakshmi-kumar, S.T. Effect of Ni doping on thick film SnO₂ gas sensor. *Sens. Actuators B Chem.* **2006**, *113*, 823–829. [[CrossRef](#)]
8. Yin, Y.; Shen, Y.; Zhou, P.; Lu, R.; Li, A.; Zhao, S.; Liu, W.; Wei, D.; Wei, K. Fabrication, characterization and n-propanol sensing properties of perovskite-type ZnSnO₃ nanospheres based gas sensor. *Appl. Surf. Sci.* **2020**, *509*, 145335. [[CrossRef](#)]
9. Wang, Z.; Miao, J.; Zhang, H.; Wang, D.; Sun, J. Hollow cubic ZnSnO₃ with abundant oxygen vacancies for H₂S gas sensing. *J. Hazard. Mater.* **2020**, *391*, 122226. [[CrossRef](#)]
10. Feng, G.Q.; Che, Y.H.; Song, C.W.; Xiao, J.K.; Fan, X.F.; Sun, S.; Huang, G.H.; Ma, Y.C. Morphology-controlled synthesis of ZnSnO₃ hollow spheres and their n-butanol gas-sensing performance. *Ceram. Int.* **2021**, *47*, 2471–2482. [[CrossRef](#)]
11. Wang, X.Y.; Zhu, X.T.; Tao, T.; Leng, B.X.; Xu, W.; Mao, L.H. Structural inheritance and change from ZnSn(OH)₆ to ZnSnO₃ compounds used for ethanol sensors: Effects of oxygen vacancies, temperature and UV on gas-sensing properties. *J. Alloys Compd.* **2020**, *829*, 154445. [[CrossRef](#)]
12. Wang, X.; Liu, Y.; Ding, B.; Li, H.; Zhu, X.; Xia, M. Influence of the addition of nano-TiO₂ and ZnO on the sensing performance of micro-ZnSnO₃ ethanol sensors under UV illumination. *Sens. Actuators B Chem.* **2018**, *276*, 211–221. [[CrossRef](#)]
13. Xun, H.; Zhang, Z.; Yu, A.; Yi, J. Remarkably enhanced hydrogen sensing of highly-ordered SnO₂-decorated TiO₂ nanotubes. *Sens. Actuators B Chem.* **2018**, *273*, 983–990. [[CrossRef](#)]
14. Shao, S.; Chen, X.; Chen, Y.; Lai, M.; Che, L. Ultrasensitive and highly selective detection of acetone based on Au@WO₃-SnO₂ corrugated nanofibers. *Appl. Surf. Sci.* **2019**, *473*, 902–911. [[CrossRef](#)]

15. Yan, Y.; Liu, J.Y.; Zhang, H.S.; Song, D.L.; Li, J.Q.; Yang, P.P.; Zhang, M.L.; Wang, J. One-pot synthesis of cubic ZnSnO₃/ZnO heterostructure composite and enhanced gas-sensing performance. *J. Alloys. Compd.* **2019**, *780*, 193–201. [[CrossRef](#)]
16. Yu, S.W.; Jia, X.H.; Yang, J.; Wang, S.Z.; Li, Y.; Song, H.J. Highly sensitive ethanol gas sensor based on CuO/ZnSnO₃ heterojunction composites. *Mater. Lett.* **2021**, *291*, 129531. [[CrossRef](#)]
17. Zhang, J.T.; Jia, X.H.; Lian, D.D.; Yang, J.; Wang, S.Z.; Li, Y.; Song, H.J. Enhanced selective acetone gas sensing performance by fabricating ZnSnO₃/SnO₂ concave microcube. *Appl. Surf. Sci.* **2021**, *542*, 148555. [[CrossRef](#)]
18. Cheng, P.; Lv, L.; Wang, Y.; Zhang, B.; Zhang, Y.; Zhang, Y.; Lei, Z.; Xu, L. SnO₂/ZnSnO₃ double-shelled hollow microspheres based high-performance acetone gas sensor. *Sens. Actuators B Chem.* **2021**, *332*, 129212. [[CrossRef](#)]
19. Chen, Y.; Yu, L.; Li, Q.; Wu, Y.; Li, Q.; Wang, T. An evolution from 3D face-centered-cubic ZnSnO₃ nanocubes to 2D orthorhombic ZnSnO₃ nanosheets with excellent gas sensing performance. *Nanotechnology* **2012**, *23*, 415501. [[CrossRef](#)]
20. Zhang, D.; Zhang, Y.; Fan, Y.; Luo, N.; Cheng, Z.; Xu, J. Micro-spherical ZnSnO₃ material prepared by microwave-assisted method and its ethanol sensing properties. *Chin. Chem. Lett.* **2020**, *31*, 2087–2090. [[CrossRef](#)]
21. Li, L.; Peng, S.; Wang, J.; Cheah, Y.L.; Teh, P.; Ko, Y.; Wong, C.; Srinivasan, M. Facile Approach to Prepare Porous CaSnO₃ Nanotubes via a Single Spinneret Electrospinning Technique as Anodes for Lithium Ion Batteries. *ACS Appl. Mater. Int.* **2012**, *4*, 6005. [[CrossRef](#)] [[PubMed](#)]
22. Qin, Y.-L.; Zhang, F.-F.; Du, X.-C.; Huang, G.; Liu, Y.-C.; Wang, L.-M. Controllable synthesis of cube-like ZnSnO₃@TiO₂ nanostructures as lithium ion battery anodes. *J. Mater. Chem. A* **2015**, *3*, 2985–2990. [[CrossRef](#)]
23. Duan, J.-F.; Hou, S.-C.; Chen, S.-G.; Duan, H.-G. Synthesis of amorphous ZnSnO₃ hollow nanoboxes and their lithium storage properties. *Mater. Lett.* **2014**, *122*, 261–264. [[CrossRef](#)]
24. Chen, O.; Wang, Y.; Wang, M.; Ma, S.; Wang, P.; Zhang, G.; Chen, W.; Jiao, H.; Liu, L.; Xu, X. Enhanced acetone sensor based on Au functionalized In-doped ZnSnO₃ nanofibers synthesized by electrospinning method. *J. Colloid Interf. Sci.* **2019**, *543*, 285–299. [[CrossRef](#)] [[PubMed](#)]
25. Lian, D.; Shi, B.; Dai, R.; Jia, X.H.; Wu, X.Y. Synthesis and enhanced acetone gas-sensing performance of ZnSnO₃/SnO₂ hollow urchin nanostructures. *J. Nanopart. Res.* **2017**, *19*, 401. [[CrossRef](#)]
26. Liu, J.; Wang, T.; Wang, B.; Sun, P.; Yang, Q.; Liang, X.; Song, H.; Lu, G. Highly sensitive and low detection limit of ethanol gas sensor based on hollow ZnO/SnO₂ spheres composite material. *Sens. Actuators B Chem.* **2017**, *245*, 551–559. [[CrossRef](#)]
27. Bai, S.L.; Tian, Y.; Zhao, Y.H.; Fu, H.; Tang, P.G.; Luo, R.X.; Li, D.Q.; Chen, A.F.; Liu, C.C. Construction of NiO@ZnSnO₃ hierarchical microspheres decorated with NiO nanosheets for formaldehyde sensing. *Sens. Actuators B Chem.* **2018**, *259*, 908–916. [[CrossRef](#)]
28. Al-Hashem, M.; Akbar, S.; Morris, P. Role of Oxygen Vacancies in Nanostructured Metal-Oxide Gas Sensors: A Review. *Sens. Actuators B Chem.* **2019**, *301*, 126845. [[CrossRef](#)]
29. Zeng, Y.; Bing, Y.-F.; Liu, C.; Zheng, W.-T.; Zou, G.-T. Self-assembly of hierarchical ZnSnO₃-SnO₂ nanoflakes and their gas sensing properties. *Trans. Nonferrous Met. Soc. China* **2012**, *22*, 2451–2458. [[CrossRef](#)]
30. Gong, H.M.; Zhao, C.H.; Niu, G.Q.; Zhang, W.; Wang, F. Construction of 1D/2D α-Fe₂O₃/SnO₂ hybrid nanoarrays for sub-ppm acetone detection. *Research* **2020**, *1*, 304–314. [[CrossRef](#)]
31. Xiao, L.; Shu, S.; Liu, S. A facile synthesis of Pd-doped SnO₂ hollow microcubes with enhanced sensing performance. *Sensors Actuators B Chem.* **2015**, *221*, 120–126. [[CrossRef](#)]